

Families of Discrete Breathers on a Nonlinear Kagome Lattice

Andrew Hofstrand

Mathematics Department, New York Institute of Technology, New York, NY 10023*

(Dated: December 11, 2024)

The unique geometry of the two-dimensional tripartite Kagome lattice is responsible for shaping diverse families of spatially localized and time-periodic nonlinear modes known as discrete breathers. We state conditions for the existence of breathers and compute their spatiotemporal profiles near the edges of the linear phonon spectrum. Our findings include the existence of strongly nonlinear and dynamically stable breathers inside the band gap, asymptotic expressions for small-amplitude breather norms, and the construction of breather families with compact support on the lattice.

The study of nonlinear waves and coherent structures on both classical and quantum lattices has a long and venerable history with diverse applications in condensed matter physics[1, 2], optical science[3, 4], mechanical metamaterials[5, 6], and circuit theory[7]. Theoretical aspects, such as the stability and localization properties of nonlinear modes, play an important role in the design of novel platforms[8]. A universal class of solutions on nonlinear lattices known as *discrete breathers*[9], which are periodic in time and spatially localized, are vital to understanding lattice dynamics with broad classes of initial data. Indeed, both transient and long-time asymptotic behavior, including energy trapping in metastable states and the transition to thermodynamic equilibrium, are intimately connected to the existence of discrete breathers on the lattice[10, 11]. Properties of discrete breathers in both conservative and damped-driven systems have been studied extensively[12], and include existence proofs, minimum energy thresholds, numerical continuation schemes, stability analyses, and the phenomena of nanoptera[13]. Unlike their continuous counterparts, the fact that the linear spectrum of the lattice is bounded makes large families of discrete breathers possible in any spatial dimension.

Two-dimensional lattices are of particular interest as toy models in physical systems due to advances in monolayer crystal fabrication in material science[14], along with applications such as trapping ultracold atoms in optical lattices[15]. Many aspects of including nonlinearity in these models are still unexplored and present novel opportunities for controlling energy localization. The Kagome lattice with its tripartite structure has recently attracted attention due to its distinct geometry[16–18], which gives rise to a bandstructure with a strictly flat band, touching one of the other dispersive bands at the Γ -point, and Dirac cones located at the corners of the hexagonal Brillouin zone (see Figure 1). The topology of the Kagome lattice is responsible for diverse phenomena such as frustrated spin dynamics in tight-binding models of magnetic systems[19], spatially compact flat-band eigenstates[20], and the existence of zero-energy modes that are pinned to the corners of a triangular lat-

tice and exhibit a generalized chiral symmetry[21–23]. Notably, due to destructive interference effects on the Kagome lattice, the latter modes remain localized even when energetically resonating with the lattice’s phonon spectrum. We consider here a well-known generalization of the Kagome lattice called the breathing Kagome (BK) lattice[24, 25], where the *intra*-unit-cell and *inter*-unit-cell coupling strengths can be unequal, reducing the lattice’s point symmetry group from C_6 to C_3 and opening a band gap at the high-symmetry points. There have been a few recent works on *nonlinear* dynamics in Kagome lattices, including a study of vortex breathers[26], a stability analysis of spatially compact breathers bifurcating from the flat-band eigenstates[27], and investigations on nonlinear corner and edge modes[28, 29].

In the current work we state conditions for the existence of discrete breathers on a nonlinear BK lattice and iteratively compute their spatiotemporal profiles, seeded from the so-called *molecular limit*[30, 31]—a simple generalization of the anti-continuum limit first introduced in [9]. After finding periodic solutions to the equations of motion on an isolated unit cell, we construct breather families on the globally-coupled lattice by tuning the inter-cell coupling strength from zero up to a value where the *fixed* breather frequency is located either just above the top band, below the bottom band, or inside the band gap of the linear phonon spectrum. Due to the diversity of features in the Kagome lattice’s dispersion relations, the continued breathers have very different localization properties, dependent on the curvature of the nearest phonon band-edges. We first construct discrete breathers inside the small phonon gap, where the band-edges approach Dirac-crossings. We show that a family of strongly nonlinear and dynamically stable soliton-like breathers exist, exhibiting a rotational sub-lattice symmetry. Next, we derive an asymptotic long-wave model for weakly-localized breathers bifurcating from the lattice’s bottom parabolic band-edge. Our asymptotic solutions provide analytic expressions for spatial norms and, through numerical continuation from the molecular limit, are shown to accurately describe how breathers terminate at band-edge. Finally, we give exact solutions for a family of compactly supported discrete breathers and numerically compute dynamically stable, symmetry-broken breathers just above the BK lattice’s flat phonon band.

* ahofstra@nyit.edu

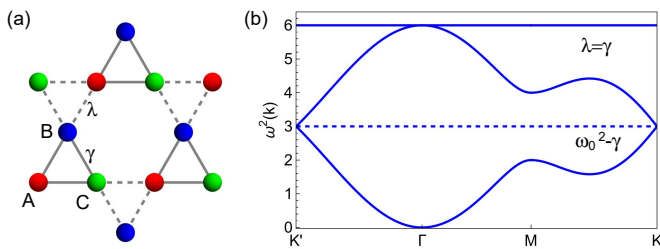


FIG. 1. (a) schematic of the BK lattice in (1); (b) phonon bands of BK lattice ($\omega_0 = 2$) when $\lambda = \gamma = 1$.

We study a nonlinear mass-spring BK lattice, shown in Figure 1(a), where the 3-site (A,B,C) unit-length equilateral triangular cell tiles the plane with lattice vectors $a_1 = (2, 0)$ and $a_2 = (1, \sqrt{3})$, indexed by $\alpha := (n, m) \in \mathbb{Z}^2$. Considering only nearest-neighbor interactions, coupled linearly, the equations of motion on the infinite lattice are

$$\begin{aligned} \ddot{x}_\alpha^A &= -V'(x_\alpha^A) + \gamma [x_\alpha^B + x_\alpha^C] + \lambda [x_{n,m-1}^B + x_{n-1,m}^C] \\ \ddot{x}_\alpha^B &= -V'(x_\alpha^B) + \gamma [x_\alpha^A + x_\alpha^C] + \lambda [x_{n,m+1}^A + x_{n-1,m+1}^C] \\ \ddot{x}_\alpha^C &= -V'(x_\alpha^C) + \gamma [x_\alpha^A + x_\alpha^B] + \lambda [x_{n+1,m}^A + x_{n+1,m-1}^B]. \end{aligned} \quad (1)$$

We take the on-site nonlinear potential V to be even and given by

$$V(z) = \frac{1}{2}\omega_0^2 z^2 + \frac{g}{2\sigma + 2}|z|^{2\sigma} z^2, \quad (2)$$

where $\sigma \in \mathbb{N}$ and $g = \pm 1$ for a *hardening* or *softening* nonlinearity, respectively. Here, the in-cell coupling γ is fixed at some positive value and the out-of-cell coupling λ is variable. The band structure of the linear lattice is depicted in Figure 1(b) in the case $\lambda = \gamma$. Notably, the top-most phonon band is flat over the entire Brillouin zone and touches the maximum of the next-lowest dispersive band at the Γ -point (this remains true when $\lambda \neq \gamma$). A band gap opens up about the Dirac cones located at the quasi-momenta K and K' and frequency $\omega_0^2 - \gamma$ when $\lambda \neq \gamma$. The width of the gap is $3|\gamma - \lambda|$ and the center of the gap is $\omega_0^2 - (\gamma + \lambda)/2$. Note that, since the matrix resulting from the linearization of system (1) about the zero solution has a constant trace, the three eigenvalues $\omega^2(k)$ at any fixed quasi-momentum k must add to $3\omega_0^2$.

The existence of discrete breathers on the globally-coupled BK lattice can be proven near the molecular limit—defined as taking $\lambda = 0$ in (1), i.e. when each unit cell is disconnected from the others. Indeed, given a non-zero, even T_b -periodic solution at the molecular limit, an application of the implicit function theorem proves the existence of a $\lambda_b > 0$ and discrete breathers on the interconnected BK lattice for $0 \leq \lambda < \lambda_b$, given that the following two mild conditions hold:

1. Non-resonance: For a breather with frequency

$\omega_b := 2\pi/T_b$, we have $(n\omega_b)^2 \neq V''(0) + \gamma$ and $(n\omega_b)^2 \neq V''(0) - 2\gamma$ for all $n \in \mathbb{Z}$.

2. Non-degeneracy: This condition is more nuanced, but holds quite broadly given that the seeded solution is even-in-time and that the derivative of the breather's period with respect to its energy is non-vanishing, $\partial T_b(E)/\partial E|_{E_*} \neq 0$ (see [9, 30] for a detailed discussion).

Satisfying the preceding conditions implies the *existence* of a $\lambda_b > 0$, but not how to obtain its optimal value. In what follows, we numerically construct breathers by expressing (1) in terms of its temporal Fourier coefficients and using a Newton-Raphson iteration scheme, seeded by a known solution in the molecular limit[30]. Our numerics suggest breathers persist until “nearly” intersecting the linear lattice’s phonon spectrum, which deforms with λ . Throughout this letter we denote the inter-cell coupling where ω_b first intersects the phonon spectrum by λ_* . Typically, once the breather frequency (or one of its higher harmonics) intersects the phonon spectrum, breathers will couple to radiating plane waves, losing localization in conservative systems like (1)[12, 30]. However in certain lattices, such as the BK lattice with its flat dispersion band, compactly localized breathers exist for $\lambda \neq 0$ (see below) and, due to destructive interference effects, cannot radiate energy via plane waves away to infinity, even if ω_b intersects the phonon bands (in this case breathers are spectrally unstable).

The molecular limit of (1) is a dynamical system with a six-dimensional phase space which admits families of quasi-periodic and possible chaotic trajectories. Here, we reduce the dimension of the phase space effectively to two by seeding the lattice with the following solutions in the molecular limit:

I C_3 symmetric states: Given $x_*^{A,B,C}(0) = a_* \neq 0$ and $\dot{x}_*^{A,B,C}(0) = 0$, there exists a periodic solution

$$\begin{pmatrix} x_*^A(t) \\ x_*^B(t) \\ x_*^C(t) \end{pmatrix} = z_*^{(I)}(t) \begin{pmatrix} 1 \\ 1 \\ 1 \end{pmatrix}$$

so long as $z_*^{(I)}$ is a periodic solution of the reduced dynamical system

$$\ddot{z} = -V'(z) + 2\gamma z, \quad z(0) = a_*, \quad \dot{z}(0) = 0.$$

II C_3 symmetry-broken states: Given $x_*^{A,B,C}(0) = a_*(1, -1, 0)^\top$ or any permutation thereof and $\dot{x}_*^{A,B,C}(0) = 0$, there exists a periodic solution

$$\begin{pmatrix} x_*^A(t) \\ x_*^B(t) \\ x_*^C(t) \end{pmatrix} = z_*^{(II)}(t) \begin{pmatrix} 1 \\ -1 \\ 0 \end{pmatrix}$$

so long as $z_*^{(II)}$ is a periodic solution of the reduced dynamical system

$$\ddot{z} = -V'(z) - \gamma z, \quad z(0) = a_*, \quad \dot{z}(0) = 0. \quad (3)$$

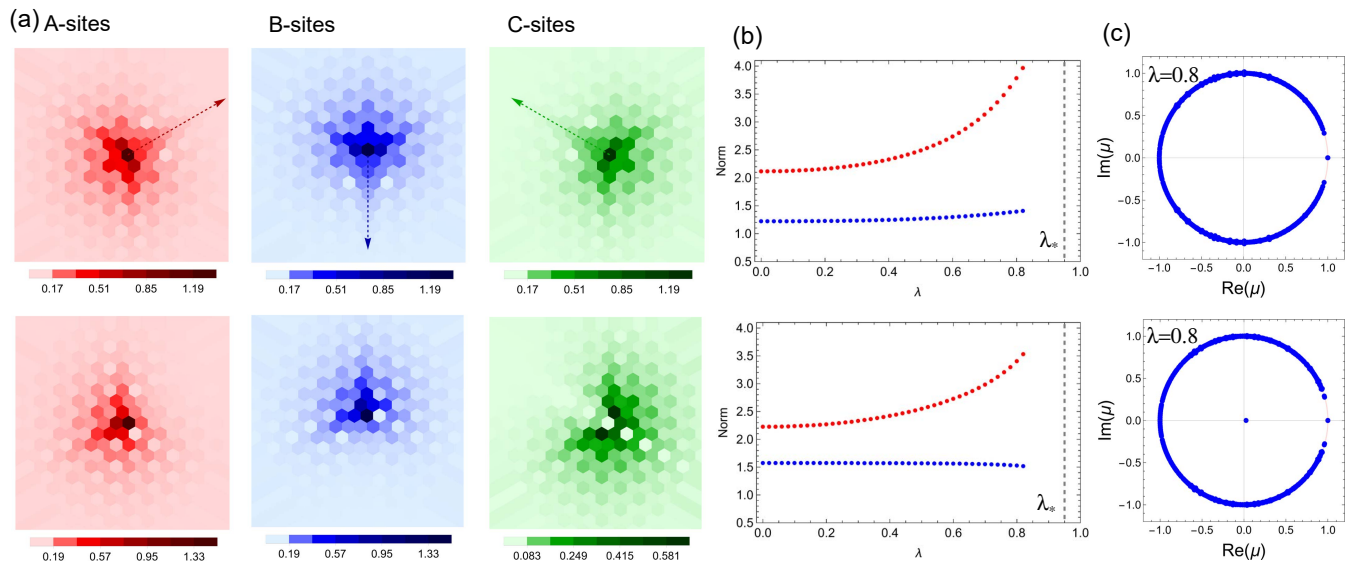


FIG. 2. **Top row of panels:** breathers with ω_b inside the phonon gap, seeded from a *symmetric* state with $g > 0$ (a) the spatial profile (absolute value) of the mid-gap breather when $\lambda = 0.8$ at $t = 0$, projected separately on its three sub-lattices (arrows highlight C_3 sub-lattice symmetry); (b) infinity- (blue) and 2- (red) norms of the breather versus inter-cell coupling ($\lambda_* = 0.95$ dashed vertical line); (c) Floquet spectrum μ of mid-gap breather shown in (a). **Bottom row of panels:** same as (a) but seeded from a *symmetry-broken* state with $g < 0$. (parameters: $\gamma, |g| = 1, \omega_0 = 2, \omega_b^2 = 3.1$).

Given the form of V , both symmetric and symmetry-broken periodic states exist, dependent on their initial amplitude a_* .

In Figure 2 we consider two breather families, each having the same frequency, ω_b , located inside the phonon band gap ($0 \leq \lambda < \lambda_*$). For the chosen parameters, when $\lambda = 0.8$, ω_b is located exactly at the center of the small phonon band gap. We seed the lattice's central unit-cell with either a symmetric state in the case of a hardening nonlinearity or a symmetry-broken state in the case of a softening nonlinearity. The respective results are displayed in the top (bottom) panels of Figure 2. In the symmetric case, the breather's C_3 sub-lattice symmetry persists onto the globally coupled lattice, as seen in the top row of Figure 2(a), where the spatial profile has been projected onto its three sub-lattice components for clarity. Similarly, the symmetry-broken breather remains so for $\lambda \neq 0$, as seen in the bottom panels of Figure 2(a). Remarkably, the symmetric family of breathers are all *dynamically stable* and both the breather amplitude and its ℓ^2 - or energy-norm grow near the band-edges, (see norms in Figure 2 (b) versus continuation parameter λ). These strongly nonlinear and localized states should be contrasted with small-amplitude discrete breathers due to tangent bifurcations from band edge plane waves[32]. Due to the Hamiltonian structure of (1), breathers are dynamically stable only if the eigenvalues of the so-called *monodromy matrix*, computed from the solution to the linearized T_b -periodic equations about the given breather, lie along the unit circle in the complex plane (Floquet multipliers)[12, 33]. The Floquet spectrum and

stability of the symmetric mid-gap breather is confirmed in the upper panel of Figure 2 (c). In contrast, the bottom panel of Figure 2 (c) shows that the corresponding symmetry-broken breather is dynamically unstable due to the single Floquet multiplier with a value greater than one along the real axis (the reciprocal of this multiplier can be seen in Figure 2(c) near zero).

Next, we consider a family of breathers having a frequency located underneath the BK lattice's lowest phonon band. As λ is increased, the parabolic band-edge at the Γ -point approaches ω_b from above. To analyze this situation, we introduce the parameter $\epsilon := \gamma/2 - \lambda$ and consider the regime $0 < \epsilon \ll 1$. Re-writing (1) in terms of the small parameter ϵ and performing a formal multiple-scale expansion in the weakly nonlinear regime yields a *focusing* nonlinear Schrödinger (NLS) equation for the breather's spatial envelope when the nonlinearity is *softening* (see end matter). Such an asymptotic analysis yields the following expressions for small-amplitude breather norms:

$$\begin{aligned} \|\{x_{n,m}^J(0)\}_{(n,m) \in \mathbb{Z}^2, J \in (A,B,C)}\|_{\ell^\infty} &\sim 2\epsilon^{1/2\sigma} \|S_0\|_{L^\infty(\mathbb{R}^2)} \\ \|\{x_{n,m}^J(0)\}_{(n,m) \in \mathbb{Z}^2, J \in (A,B,C)}\|_{\ell^2}^2 &\sim 2\sqrt{3}\epsilon^{(1-\sigma)/\sigma} \|S_0\|_{L^2(\mathbb{R}^2)}^2, \end{aligned} \quad (4)$$

where $S_0(Z, H)$ is the radial ground-state solitary wave solution of the derived NLS equation and can be obtained numerically[34]. Our asymptotic expressions for the norms are shown by the solid curves in Figure 3 for two different nonlinearity strengths ($\sigma = 1, 2$) and agree well with the computed breather norms, continued from

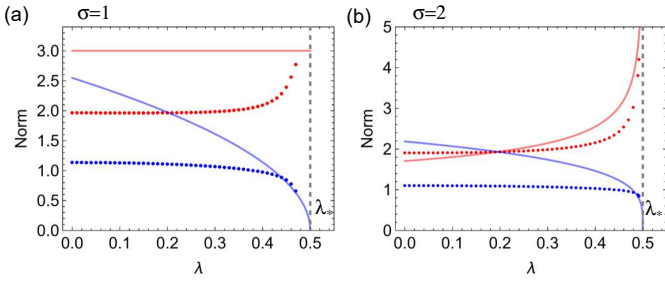


FIG. 3. Infinity- (blue dots) and 2- (red dots) norms of breather family with ω_b located below the bottom phonon band, continued from a symmetric state in the molecular limit for $g < 0$ when (a) $\sigma = 1$ and (b) $\sigma = 2$. Solid curves indicate the corresponding asymptotic norms calculated from the expressions given in the text, showing agreement as $\lambda \rightarrow \lambda_*$. (parameters: $g = -1$, $\omega_b = 1$, $\lambda_* = 0.5$).

the distant molecular limit, near the band-edge as λ approaches λ_* . In the case of cubic nonlinearity, $\sigma = 1$, the ℓ^2 -scaling is *critical*, meaning that breathers bifurcating from the zero solution exist only above a certain nonzero energy threshold, which is indicated with the solid horizontal line in Figure 3(a). This energy threshold becomes infinite when considering the *super-critical* case, $\sigma = 2$, shown in Figure 3(b).

Finally, as a result of the flat phonon band[35], the BK lattice admits families of discrete breathers with compact support. An explicit solution of this type is supported on

six lattice sites of a closed hexagonal ring, given by

$$\begin{aligned} x_{0,0}^A &= x_{-1,1}^C = x_{-1,0}^B = z^{(II)}(t), \\ x_{0,0}^B &= x_{-1,1}^A = x_{-1,0}^C = -z^{(II)}(t), \\ x_{n,m}^J &\equiv 0 \text{ for all other } (n,m) \in \mathbb{Z}^2, \end{aligned}$$

where $z^{(II)}(t)$ is a T_b -periodic solution to the initial value problem (3) with γ replaced by $\gamma + \lambda$. The symmetric spatial profile is depicted in the top panels of Figure 4(a). In the case of a cubic nonlinearity, (3) is completely integrable and its solution is expressed in terms of Jacobi elliptic functions with a period given explicitly by

$$T_b = \frac{4}{\sqrt{s + ga_*^2}} \mathcal{K} \left(\sqrt{\frac{ga_*^2}{2(s + ga_*^2)}} \right), \quad (5)$$

where $s := \omega_0^2 + \lambda + \gamma$ and \mathcal{K} is the complete elliptic integral of the first kind[36]. Similar compact breathers were obtained in a discrete nonlinear Schrodinger (dNLS) model of a Kagome lattice in [27].

In Figure 4 we consider breathers having a frequency above the flat phonon band and $g > 0$. Using (5), the solid curves in Figure 4(b) show the breather's spatial norms versus λ . A dynamically stable breather bifurcates from the zero solution at the flat phonon band ($\lambda = \lambda_*$) with a zero-energy threshold (in contrast to those, for instance, in Figure 3), and at the molecular limit, $\lambda = 0$, the (unstable) breather consists of *three* symmetry

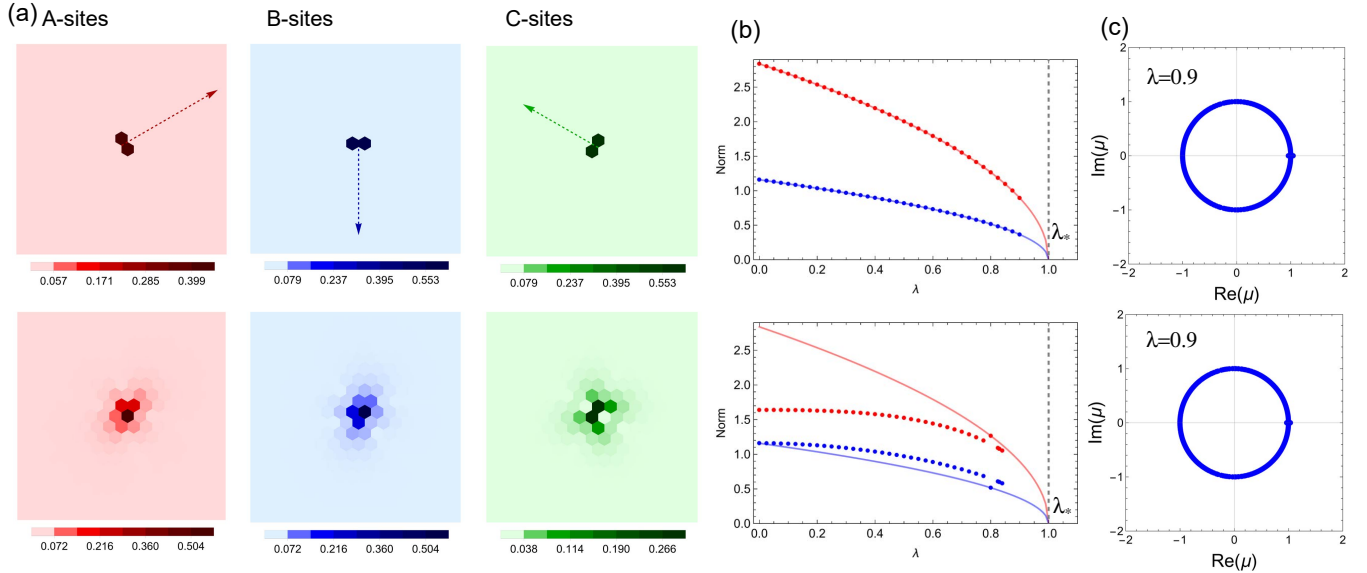


FIG. 4. **Top row of panels:** six-site compact breather with ω_b above flat phonon band (a) absolute spatial profile when $\lambda = 0.9$ (arrows highlight C_3 sub-lattice symmetry); (b) infinity- (blue dots) and 2- (red dots) norms computed from molecular limit discussed in the text and solid curves are the exact norms obtained from (5) ($\lambda_* = 1$ dashed vertical line); (c) Floquet spectrum μ of breather near λ_* . **Bottom row of panels:** same as top row but seeded from a *single* symmetry-broken state, where the solid curves in the bottom panel of (b) are copied from the top panel for reference. (parameters: $g = 1$, $\omega_b = 6$).

-broken states arranged along a hexagonal ring. In the bottom panels of Figure 4 we explicitly break the C_3 sub-lattice symmetry by seeding the continuation scheme with a *single* symmetry-broken state in the molecular limit. The resulting nontrivial family of symmetry-broken breathers exhibit extreme localization on the globally coupled lattice, becoming dynamically stable in the weakly nonlinear regime as λ approaches λ_* (see Figure 4(c)). Addressing the stability-switching and localization properties of these nonlinear modes near the flat band is an open avenue for further research.

In this letter, we have shown that the unique geometry

of the Kagome lattice offers a novel means to shape diverse families of discrete breathers and precisely control energy localization via nonlinearity and easily tunable parameters in physical systems.

ACKNOWLEDGEMENTS

This work was supported by the Air Force Office of Scientific Research with Grant No. FA9550-23-1-0144 and the Simons Foundation collaboration “Harnessing Universal Symmetry Concepts for Extreme Wave Phenomena.”

-
- [1] O. M. Braun and Y. S. Kivshar, *Frenkel Kontorova Model: Concepts, Methods, and Applications* (Springer, 2010).
- [2] O. Morsch and M. Oberthaler, Dynamics of bose-einstein condensates in optical lattices, *Rev. Mod. Phys.* **78** (2006).
- [3] J. V. Moloney and A. C. Newell, *Nonlinear Optics* (CRC Press LLC, 2003).
- [4] A. Blanco-Redondo, C. M. de Sterke, C. Xu, S. Wabnitz, and S. K. Turitsyn, The bright prospects of optical solitons after 50 years, *Nature Photonics* **17** (2023).
- [5] K. Bertoldi, V. Vitelli, J. Christensen, and M. van Hecke, Flexible mechanical metamaterials, *Nature Reviews Materials* **2** (2017).
- [6] Y. Zhang, B. Li, Q. S. Zheng, G. M. Genin, and C. Q. Chen, Programmable and robust static topological solitons in mechanical metamaterials, *Nature Communications* **10** (2019).
- [7] Y. Hadad, J. C. Soric, A. B. Khanikaev, and A. Alu, Self-induced topological protection in nonlinear circuit arrays, *Nature Electronics* **1** (2018).
- [8] H. Li, A. Hofstrand, and M. I. Weinstein, Stability of traveling waves in a nonlinear hyperbolic system approximating a dimer array of oscillators, arXiv <https://doi.org/10.48550/arXiv.2402.07567> (2024).
- [9] R. S. MacKay and S. Aubry, Proof of existence of breathers for time-reversible or hamiltonian networks of weakly coupled oscillators., *Nonlinearity* **7** (1994).
- [10] N. J. Zabusky, Z. Sun, and G. Peng, Measures of chaos and equipartition in integrable and nonintegrable lattices, *Chaos* **16** (2006).
- [11] D. A. Caballero and C. E. Wayne, Damped and driven breathers and metastability, arXiv <https://doi.org/10.48550/arXiv.2101.10999> (2022).
- [12] S. Flach and A. V. Gorbach, Discrete breathers—advances in theory and applications, *Phys. Rep.* **467** (2008).
- [13] C. J. Lustri and M. A. Porter, Nanoptera in a period-2 toda chain, *SIAM Journal on Applied Dynamical Systems* **17** (2018).
- [14] C. Liu, T. Liu, Z. Zhang, Z. Sun, G. Zhang, E. Wang, and K. Liu, Understanding epitaxial growth of two-dimensional materials and their homostructures, *Nature Nanotechnology* (2024).
- [15] G.-B. Jo, J. Guzman, C. K. Thomas, P. Hosur, A. Vishwanath, and D. M. Stamper-Kurn, Ultracold atoms in a tunable optical kagome lattice, *Physical Review Letters* **108** (2012).
- [16] J.-X. Yin, B. Lian, and M. Z. Hasan, Topological kagome magnets and superconductors, *Nature* **612** (2022).
- [17] M. Fruchart, Y. Zhou, and V. Vitelli, Dualities and non-abelian mechanics, *Nature* **577** (2020).
- [18] M. Li, D. Zhirihin, M. Gorlach, X. Ni, D. Filonov, A. Slobozhanyuk, A. Alu, and A. B. Khanikaev, Higher-order topological states in photonic kagome crystals with long-range interactions, *Nature Photonics* **14** (2020).
- [19] K. Hoffhuis, S. H. Skjaervo, S. Parchenko, H. Arava, Z. Luo, A. Kleibert, P. M. Derlet, and L. J. Heyderman, Real-space imaging of phase transitions in bridged artificial kagome spin ice, *Nature Physics* **18** (2022).
- [20] D. L. Bergman, C. Wu, and L. Balents, Band touching from real-space topology in frustrated hopping models, *Physical Review B* **78** (2008).
- [21] X. Ni, M. Weiner, A. Alu, and A. B. Khanikaev, Observation of higher-order topological acoustic states protected by generalized chiral symmetry, *Nature Materials* **18** (2019).
- [22] M. A. J. Herrera, S. N. Kempkes, M. B. de Paz, A. García-Etxarri, I. Swart, C. M. Smith, and D. Bercioux, Corner modes of the breathing kagome lattice: Origin and robustness, *Physical Review B* **105** (2022).
- [23] Z. Wang, X. Wang, Z. Hu, D. Bongiovanni, D. Jukić, L. Tang, D. Song, R. Morandotti, Z. Chen, and H. Buljan, Sub-symmetry-protected topological states, *Nature Physics* **19** (2023).
- [24] M. Ezawa, Higher-order topological insulators and semimetals on the breathing kagome and pyrochlore lattices, *Physical Review Letters* **120** (2018).
- [25] T. H. Barter, T.-H. Leung, M. Okano, M. Block, N. Y. Yao, and D. M. Stamper-Kurn, Spatial coherence of a strongly interacting bose gas in the trimerized kagome lattice, *Physical Review A* **101** (2020).
- [26] K. J. H. Law, A. Saxena, P. G. Kevrekidis, and A. R. Bishop, Localized structures in kagome lattices, *Physical Review A* **79** (2009).
- [27] R. A. Vicencio and M. Johansson, Discrete flat-band solitons in the kagome lattice, *Physical Review A* **87** (2013).

- [28] M. S. Kirsch, Y. Zhang, M. K. Lukas, J. Maczewsky, S. K. Ivanov, Y. V. Kartashov, L. Torner, D. Bauer, A. Szameit, and M. Heinrich, Nonlinear second-order photonic topological insulators, *Nature Physics* **17** (2021).
- [29] K. Prabith, G. Theocharis, and R. Chaunsali, Nonlinear corner states in topologically nontrivial kagome lattices, arXiv <https://arxiv.org/abs/2404.02504> (2024).
- [30] A. Hofstrand, H. Li, and M. I. Weinstein, Discrete breathers of nonlinear dimer lattices: bridging the anti-continuous and continuous limits, *Journal of Nonlinear Science* **33** (2023).
- [31] F. Schindler, V. B. Bulchandani, and W. B. Benalcazar, Nonlinear breathers with crystalline symmetries, arXiv <https://doi.org/10.48550/arXiv.2309.07244> (2023).
- [32] S. Flach, Tangent bifurcation of band edge plane waves, dynamical symmetry breaking and vibrational localization, *Physica D* **91** (1996).
- [33] T. Kapitula and K. Promislow, *Spectral and Dynamical Stability of Nonlinear Waves* (Springer, 2013).
- [34] G. Fibich, *The Nonlinear Schrodinger Equation: Singular Solutions and Optical Collapse* (Springer, 2015).
- [35] C. Danieli, A. Maluckov, and S. Flach, Compact discrete breathers on flat-band networks, *Low Temp. Phys.* **44**

(2018).

- [36] M. Abramowitz and I. Stegun, *Handbook of Mathematical Functions* (Dover, 1980).

Appendix A: Multiple-scale derivation of weakly nonlinear breather envelopes near bottom phonon band

Here, we outline the derivation of the asymptotic expressions for breather norms stated in (4). First, using the parameter $\epsilon = \gamma/2 - \lambda$, we re-scale coordinates, $x_{n,m}^J = \epsilon^{1/2\sigma} Y_{n,m}^J$, and express system (1) in terms of ϵ and $Y_{n,m}^J$. Taking the continuum limit[30], we introduce $u_J(t, \zeta, \eta) \sim Y_{n,m}^J(t)$, with continuous spatial variables ζ and η . Due to the parabolic behavior of the bottom dispersion band near Γ , we truncate the resulting Taylor series at second-order, and (1) becomes the following system of PDEs:

$$\begin{aligned} \partial_t^2 u_A &= -\omega_0^2 u_A - g\epsilon u_A^{2\sigma+1} + \gamma \left[\frac{3}{2} u_B - \frac{\sqrt{3}}{2} \partial_\eta u_B + \frac{3}{4} \partial_\eta^2 u_B - \frac{1}{2} \partial_\zeta u_B + \frac{\sqrt{3}}{2} \partial_\zeta \partial_\eta u_B + \frac{1}{4} \partial_\zeta^2 u_B + \frac{3}{2} u_C - \partial_\zeta u_C + \partial_\zeta^2 u_C \right] \\ &\quad - \epsilon \left[u_B - \sqrt{3} \partial_\eta u_B + \frac{3}{2} \partial_\eta^2 u_B - \partial_\zeta u_B + \sqrt{3} \partial_\zeta \partial_\eta u_B + \frac{1}{2} \partial_\zeta^2 u_B + u_C - 2\partial_\zeta u_C + 2\partial_\zeta^2 u_C \right] \\ \partial_t^2 u_B &= -\omega_0^2 u_B - g\epsilon u_B^{2\sigma+1} + \gamma \left[\frac{3}{2} u_A + \frac{\sqrt{3}}{2} \partial_\eta u_A + \frac{3}{4} \partial_\eta^2 u_A + \frac{1}{2} \partial_\zeta u_A + \frac{\sqrt{3}}{2} \partial_\zeta \partial_\eta u_A + \frac{1}{4} \partial_\zeta^2 u_A + \frac{3}{2} u_C + \frac{\sqrt{3}}{2} \partial_\eta u_C + \frac{3}{4} \partial_\eta^2 u_C \right. \\ &\quad \left. - \frac{1}{2} \partial_\zeta u_C - \frac{\sqrt{3}}{2} \partial_\zeta \partial_\eta u_C + \frac{1}{4} \partial_\zeta^2 u_C \right] - \epsilon \left[u_A + \sqrt{3} \partial_\eta u_A + \frac{3}{2} \partial_\zeta^2 u_A + \partial_\zeta u_A + \sqrt{3} \partial_\zeta \partial_\eta u_A + \frac{1}{2} \partial_\zeta^2 u_A + u_C + \sqrt{3} \partial_\eta u_C \right. \\ &\quad \left. + \frac{3}{2} \partial_\eta^2 u_C - \partial_\zeta u_C - \sqrt{3} \partial_\eta \partial_\zeta u_C + \frac{1}{2} \partial_\zeta^2 u_C \right] \\ \partial_t^2 u_C &= -\omega_0^2 u_C - g\epsilon u_C^{2\sigma+1} + \gamma \left[\frac{3}{2} u_A + \partial_\zeta u_A + \partial_\zeta^2 u_A + \frac{3}{2} u_B - \frac{\sqrt{3}}{2} \partial_\eta u_B + \frac{3}{4} \partial_\eta^2 u_B + \frac{1}{2} \partial_\zeta u_B - \frac{\sqrt{3}}{2} \partial_\zeta \partial_\eta u_B + \frac{1}{4} \partial_\zeta^2 u_B \right] \\ &\quad - \epsilon \left[u_A + 2\partial_\zeta u_A + 2\partial_\zeta^2 u_A + u_B - \sqrt{3} \partial_\eta u_B + \frac{3}{2} \partial_\eta^2 u_B + \partial_\zeta u_B - \sqrt{3} \partial_\zeta \partial_\eta u_B + \frac{1}{2} \partial_\zeta^2 u_B \right]. \end{aligned}$$

For $0 < \epsilon \ll 1$, we define the long spatiotemporal independent scales:

$$Z = \sqrt{\epsilon} \zeta, H = \sqrt{\epsilon} \eta, \text{ and } T = \epsilon t,$$

and expand in powers of $\sqrt{\epsilon}$:

$$u_J(t, T, \zeta, Z, \eta, H) = u_J^{(0)} + \sqrt{\epsilon} u_J^{(1)} + \epsilon u_J^{(2)} + \dots$$

At zeroth-order:

$$\mathcal{L} \begin{pmatrix} u_A^{(0)} \\ u_B^{(0)} \\ u_C^{(0)} \end{pmatrix} = 0,$$

where

$$\mathcal{L} = (\partial_t^2 + \omega_0^2) \mathcal{I}_{3 \times 3} - \frac{3}{2} \gamma \begin{pmatrix} 0 & 1 & 1 \\ 1 & 0 & 1 \\ 1 & 1 & 0 \end{pmatrix} + \frac{1}{2} \gamma \begin{pmatrix} 0 & \sqrt{3} \partial_\eta + \partial_\zeta & 2 \partial_\zeta \\ -\sqrt{3} \partial_\eta - \partial_\zeta & 0 & -\sqrt{3} \partial_\eta + \partial_\zeta \\ -2 \partial_\zeta & \sqrt{3} \partial_\eta - \partial_\zeta & 0 \end{pmatrix} \\ - \frac{1}{4} \gamma \begin{pmatrix} 0 & (\sqrt{3} \partial_\eta + \partial_\zeta)^2 & 4 \partial_\zeta^2 \\ (\sqrt{3} \partial_\eta + \partial_\zeta)^2 & 0 & (\sqrt{3} \partial_\eta - \partial_\zeta)^2 \\ 4 \partial_\zeta^2 & (\sqrt{3} \partial_\eta - \partial_\zeta)^2 & 0 \end{pmatrix},$$

and where $\mathcal{I}_{3 \times 3}$ is the identity matrix.

We look for solutions to the zeroth-order system in the form:

$$u^{(0)}(t, T, \zeta, Z, \eta, H) = R(T, Z, H) v e^{i\omega t} + c.c.$$

for nonzero $v \in \mathbb{C}^3$, where *c.c.* denotes complex conjugate of the term preceding it. Substituting and solving leads to the orthonormal eigensystem:

$$\omega_-^2 := \omega_0^2 - 3\gamma \quad \text{and} \quad v_- := \frac{1}{\sqrt{3}} \begin{pmatrix} 1 \\ 1 \\ 1 \end{pmatrix} \\ \omega_+^2 := \omega_0^2 + \frac{3}{2}\gamma \quad \text{and} \quad v_{+,1 \setminus 2} := \frac{1}{\sqrt{2}} \begin{pmatrix} -1 \\ 0 \\ 1 \end{pmatrix}, \quad \frac{1}{\sqrt{2}} \begin{pmatrix} -1 \\ 1 \\ 0 \end{pmatrix}.$$

Here, we are interested in breathers with fixed frequency $\omega_b = \omega_-$ and so consider zeroth-order solutions in the form

$$u^{(0)} = R(T, Z, H) \sqrt{3} v_- e^{i\omega_- t} + c.c.$$

$$\mathcal{L} \begin{pmatrix} u_A^{(2)} \\ u_B^{(2)} \\ u_C^{(2)} \end{pmatrix} = \left[\left(-2i\omega_- \partial_T R - g \binom{2\sigma+1}{\sigma} |R|^{2\sigma} R - 2R \right) \sqrt{3} v_- + \frac{\gamma}{12} \partial_Z^2 R \begin{pmatrix} 11 \\ 2 \\ 11 \end{pmatrix} - \frac{\sqrt{6}\gamma}{2} \partial_Z \partial_H R v_{+,1} + \frac{\gamma}{12} \partial_H^2 R \begin{pmatrix} 5 \\ 14 \\ 5 \end{pmatrix} \right] e^{i\omega_- t} \\ + \text{non-resonant terms} + c.c.,$$

where the coefficient to the nonlinear term is a binomial coefficient.

By taking the orthogonal projection of the above right-hand-side onto v_- and forcing the resonant terms to vanish leads to the following NLS equation:

$$-2i\omega_- \partial_T R - g \binom{2\sigma+1}{\sigma} |R|^{2\sigma} R - 2R + \frac{2}{3} \gamma \Delta R = 0 \quad (\text{A1})$$

For a softening nonlinearity, $g = -1$, the NLS equation

At first-order:

$$\mathcal{L} \begin{pmatrix} u_A^{(1)} \\ u_B^{(1)} \\ u_C^{(1)} \end{pmatrix} = \gamma \begin{pmatrix} -\frac{3}{2} \partial_Z R - \frac{\sqrt{3}}{2} \partial_H R \\ \sqrt{3} \partial_H R \\ \frac{3}{2} \partial_Z R - \frac{\sqrt{3}}{2} \partial_H R \end{pmatrix} e^{i\omega_- t} + c.c.$$

The right-hand-side of the above equation can be expressed

$$\frac{\sqrt{2}}{2} \gamma \left(3v_{+,1} \partial_Z R + \sqrt{3} (2v_{+,2} - v_{+,1}) \partial_H R \right) e^{i\omega_- t} + c.c.$$

Since the operator \mathcal{L} is self-adjoint and the expression above is contained in the orthogonal complement of \mathcal{L} 's kernel, the Fredholm alternative implies the system's solvability. Indeed, a particular solution, $u_p^{(1)}$, of the first-order system is given by a constant multiple of the above expression:

$$u_p^{(1)} = \frac{\sqrt{2}}{3} \left(v_{+,1} \partial_Z R + \frac{1}{\sqrt{3}} (2v_{+,2} - v_{+,1}) \partial_H R \right) e^{i\omega_- t} + c.c.$$

Plugging in the zeroth and first order solutions gives at second-order:

above is of ‘‘focusing’’ type and has spatially localized solitary wave solutions. We seek solutions of the form

$$R(T, Z, H) = S(Z, H; \nu) e^{i\nu T/2\omega_-}$$

which gives the asymptotic solutions on the BK lattice:

$$\begin{pmatrix} x_{n,m}^A(t) \\ x_{n,m}^B(t) \\ x_{n,m}^C(t) \end{pmatrix} \sim 2\epsilon^{1/2\sigma} S(\sqrt{\epsilon} n, \sqrt{\epsilon} m; \nu) \begin{pmatrix} 1 \\ 1 \\ 1 \end{pmatrix} \cos \left(\left[\omega_- + \frac{\nu \epsilon}{2\omega_-} \right] t \right). \quad (\text{A2})$$

We can then use (A2) to compute the spatial norms of the small-amplitude breathers stated in (4). The constant term in the second expression in (4) is due to the area of the hexagonal Voronoi cell of the Kagome lattice. In spatial dimensions greater than one, the ground-state

radial solitary wave solution of the focusing NLS, S_0 , is not given explicitly, but can be found numerically. Here we use the *spectral renormalization method*[34] (In Figure 3 we use $\|S_0\| \approx 1.61$ for $\sigma = 1$ and $\|S_0\| \approx 0.77$ for $\sigma = 2$).